Aromatic Polyamide Brushes for High Young's Modulus Surfaces by Surface Initiated Chain-Growth Condensation Polymerization

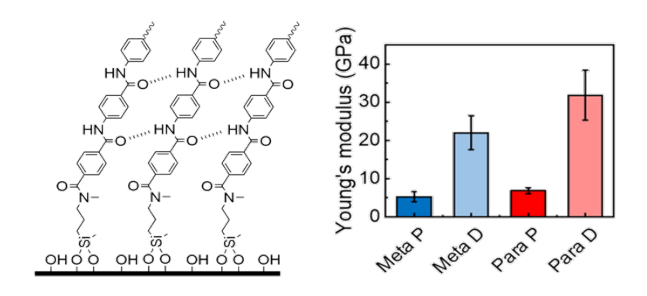
Caleb J. Reese[†], Yarong Qi[‡], Dustin T. Abele[†], Maximillian D. Shlafstein[†], Rhys J. Dickhudt[†],

Xun Guan[‡], Michael J. Wagner[†], Xitong Liu^{*‡}, Stephen G. Boyes^{*,†}

†Department of Chemistry, The George Washington University, Washington, DC 20052, USA

*Department of Civil & Environmental Engineering, The George Washington University,
Washington, DC 20052, USA

Keywords: Polymer brushes, Rigid rod brushes, Hydrogen bonding brushes, Aromatic polyamides



Abstract

Since being developed over 50 years ago, aromatic polyamides have been used industrially for numerous high-performance applications due to their heat resistance, chemical stability, and high strength. Despite this extensive time span, few applications as surface coatings have been explored due to most aromatic polyamides being insoluble in organic solvents and their extremely high melting temperatures. However, new polymerization techniques have been developed to overcome this insolubility allowing applications such as reverse osmosis membranes and gas separation membranes to be developed. With the recent advancement of substituent effect chain growth condensation polymerization, controlled growth aromatic polyamides have been shown to grow from flat and curved surfaces. In this study aromatic polyamides with a protecting side chain were grown from flat and curved surfaces to allow for deprotection post polymerization and the introduction of hydrogen bonding along the backbone of the polyamide. The aromatic polyamide brushes formed were then characterized using TEM and AFM to explore important physical properties of the polymer brushes, including grafting density and Young's modulus. The introduction of hydrogen bonding dramatically increased the Young's modulus of the polyamide brushes from 5-6 GPa to 22-32 GPa. Our results demonstrate the tunability of the aromatic polyamide brushes to achieve high mechanical strength and pave the way for their application in areas such as high-performance coatings.

Introduction

Aromatic polyamides have long been known to possess excellent chemical and thermal stability, and superior mechanical properties.¹ These properties primarily stem from their rod-like aromatic amide linkage and the hydrogen bonding that occurs along the backbone. These properties have led to aromatic polyamides fibers being used in many high-performance applications including

protective clothing, bullet-proof body armor, composites for armament and aerospace applications, composites for asbestos substitutes, and high-temperature insulation paper.² While many studies have been performed to understand bulk semi-crystalline aromatic polyamide fibers, there have been limited investigations into high performance aromatic polyamide films due to the lack of techniques needed to produce well-defined surface coatings of these polymers.^{3,4} This is primarily due to the step-growth polymerization technique typically required to synthesize aromatic polyamides, which makes modification of surfaces to produced well-defined coatings difficult. Despite this hurdle, aromatic polyamide coatings have been extensively used for reverse osmosis (RO) membranes due to their excellent performance and have been recently used in gas separation membranes.⁵⁻⁸ While these applications are very important, the films used tend to suffer from coating instability and often do not exhibit the predicted physical properties of aromatic polyamides due to the non-covalent attachment of the polymers to the surface, the lack of control over the coating properties, and limitations introduced by chemical modifications made to improve polymer solubility in adapting the aromatic polyamides for these applications.^{8,9}

The development of well-defined, covalently attached polymer coatings prepared from semi-rigid or rigid-rod polymers has recently attracted significant attention, as highlighted in a recent review published by our group. Many theoretical studies have predicted these systems would possess advantageous properties, such as strong orientation order, weak interpenetration, strong interfacial tension, semi-crystalline properties, and exceptional long-range order. One of the factors limiting the expansion of these systems is the identification of suitable synthetic techniques to prepare the well-defined coatings. This is particularly evident with aromatic polyamide systems. Typically, two methods have been used to make covalently attached aromatic polyamide films, molecular layer deposition (MLD) and molecular layer by layer deposition (mLbL). MLD and

mLbL typically use two different monomers possessing acid chloride groups on one and amine groups on the other monomer, where the acid chlorides react with the amines to form the amide linkage. In each case, one monomer is reacted on the surface until complete saturation has occurred. This is followed by a purge and/or rinse period to remove the unreacted monomer. The next monomer is then added to the system to continue growth of the polymer coating, followed by another purge and/or rinse cycle. The monomers reacting with the surface are then alternated until the desired thickness is achieved. The primary difference between the two techniques is that MLD is performed in the vapor phase, whereas mLbL is conducted in the solution phase. 19,21 Because of the low volatility of most aromatic polyamide monomers, the mLBL technique is more commonly used.^{17-20,22-29} While these methods have been successfully used to produce aromatic polyamide thin films, they both have issues with variability of growth rate, long polymerization times, limited thickness, and self-limiting growth. 17-20 Because of the challenges associated with MLD and mLbL, recently our group reported on a new surface-initiated polymerization technique that could allow for the preparation of well-defined, covalently attached aromatic polyamide brush films using a one-step polymerization.³⁰

Polymer brushes are polymers chains that are attached to a surface with a high enough grafting density to force the chains to adopt an extended conformation away from the surface.³⁰ Polymer brushes have played an important role in the area of surface modification due to the high level of control over surface properties they offer, and the ability to make covalently attached films with a variety of different functionalities and topographies.^{31,32} Traditionally polymer brushes have been made primarily using vinyl-based monomers due to the need for a chain-growth mechanism to produce well-defined coatings. This requirement limited the opportunities of producing polymer brushes from polymers normally synthesized using a step-growth mechanism, such as aromatic

polyamides. However, recently our group demonstrated the growth of densely grafted aromatic polyamide brushes from both flat and curved silica surfaces.³⁰ To make these polymer brushes the traditional step-growth polymerization to produce aromatic polyamides had to be converted to a chain-growth polymerization. This conversion was performed using a solution-based technique developed by Yokozawa et al. that focused on substituent effect chain-growth condensation (CGC) polymerization.³³⁻³⁷ Yokozawa hypothesized this technique works using a "deactivated" monomer and an "activated" initiator to favor reaction of the monomer with the propagation chain instead of monomer reacting with itself, resulting in a chain-growth process.³⁸⁻⁴³ Subsequent work from our group found that, in addition to the activation-deactivation roles of the monomer and initiator, the pK_a of the monomer leaving group also plays a critical role in establishing the CGC polymerization kinetics and in producing well-defined polymers.^{44,45} Adaptation of the solution-based substituent effect CGC polymerization method to a surface-initiated technique led to the preparation of well-defined and uniform polymer brushes from silica surfaces.³⁰

While our original work was the first report of the synthesis of well-defined aromatic polyamide brushes using substituent effect CGC polymerization, application of the polymer synthesized was limited due to the presence of an octyl side chain on the nitrogen of the polyamide linkage. This side chain was used, both in our work and the solution work by Yokozawa, to help with solubility of the polymer and limit side reactions during the polymerization. Aromatic polyamides alone with many other rigid rod polymers typically have very low solubility in most solvents making them difficult to synthesize and characterize. Because of this, aromatic polyamides are industrially synthesized with solvents such as N-methyl-2-pyrrolidone and extruded into fibers using sulfuric acid. As such, in order to synthesize well-defined aromatic polyamides using the substituent effect CGC polymerization technique, a solubilizing side chain is used to allow for

polymers of reasonable molecular weight and the use of lower boiling point solvents, such as tetrahydrofuran (THF). However, the exceptional physical properties of aromatic polyamides primarily come from the packing of the rigid aromatic polymer backbone and the hydrogen bonding between the amide linkages, both of which are disrupted when using a solubilizing side chain. To overcome this issue in solution-based polymerizations, Yokozawa reported the use of a nitrogen protection strategy using a benzyl ether side chain that could be removed after the polymerization was complete.³⁴ This protecting side chain allows for polymerizations of higher molecular weight polymers at lower polymerization temperatures using conventional polymerization solvents. Once the polymers are formed, the protecting side chain is cleaved, producing an amide proton which can then hydrogen bond with neighboring chains and allow tighter packing of the polymer chains to produce the high-performance properties associated with aromatic polyamides.

In this report the use of a protection strategy, inspired by Yokozawa's solution polymerizations, to make high performance aromatic polyamide brushes is presented. In addition to the brush synthesis, optimization of the polymerization kinetics and brush properties, compared to our previous study, was performed.³⁰ A new surface initiator was used to enable fast initiation relative to propagation, which allowed for the preparation of well-defined brushes of controlled molecular weight and narrow molecular weight distribution.⁴⁵ The effect of monomer structure on the polymerization kinetics and brush properties was also investigated by using both para- and metasubstituted monomers. Protected aromatic polyamide brushes were grown using a surface-initiated substituent effect CGC polymerization on both high surface area Stöber silica particles and flat silica wafers. The deprotection strategy was then used to cleave the side chain allowing for hydrogen bonding along the backbone of the rigid-rod like aromatic polyamide brushes. The final

polymer brushes were characterized using transmission electron microscope (TEM), goniometry, ellipsometry, and atomic force microscopy (AFM) to better characterize the improved surface properties.

Experimental section

Materials. All chemicals were purchased from Sigma Aldrich and were used as received unless otherwise noted. N-methylaminopropylmethyldimethoxysilane was purchased from Gelest and used as received. HPLC grade THF and HPLC grade toluene were purified and dispensed through a MBRAUN MB-SPS solvent purification system. Silicon wafers (prime grade, single side polished) were obtained from Wafer World, with only a native oxide.

Characterization. ¹H and ¹³C nuclear magnetic resonance (NMR) spectra were obtained using an Agilent 400-MR DD2 NMR spectrometer. Ellipsometry measurements were carried out on a FS-1 Film Sense multi-wavelength ellipsometer with a 65° angle of incidence. Refractive indices and thickness were measured using a Cauchy model. Infrared spectra were recorded using a Perkin-Elmer Frontier Fourier-transform infrared (FTIR) spectroscopy spectrometer using a diamond/ZnSe attenuated total reflectance (ATR) crystal for bulk samples, and a Harrick Scientific VariGATR (grazing-angle ATR) accessory for thin films on silicon wafers. Contact angle measurements were recorded with a ramé-hart standard goniometer 260-U4 using 10 μL drops of deionized water. Images were captured using DROPImage software. A FEI Talos 200 kV with a field-emission source was used to obtain TEM micrographs. Samples were prepared by dispersing a small amount of material into THF assisted by sonic agitation. An approximately 2 μL aliquot of the mixture was dispersed on a carbon coated 400 mesh copper grid and allowed to dry for 2 h under vacuum before inserting into the TEM. Thermogravimetric analysis (TGA) was performed on a Perkin-Elmer PYRIS 1 TGA. The samples were placed in a platinum crucible, and then heated

in air at a ramp rate of 20 °C/min. Number average molecular weight (M_n) and polydispersity index (PDI) were measured using a Wyatt miniDawn, Wyatt Optilab, and Agilent HPLC gel-permeation chromatography (GPC) unit (eluent: inhibitor free THF with a flow rate of 1.0 mL/min using 5 µm PSS SDV Lux analytical columns: molecular weight range 100-10,000 (1000 A) and 1,000-1,000,000 (100,000 A) g/mol (polystyrene equivalent), respectively). A dn/dc value for the prepared polymers of 0.16 for THF and 0.13 for chloroform was determined and used during the analysis. An atomic force microscope (MultiMode 8-HR, Bruker Inc.) was used to characterize the topography and roughness of samples using a ScanAsyst – Air probe. RTESPA-525 and RTESPA-525-30 probes were used to perform Young's modulus measurement under the force volume mode. The RTESPA-525-30 (nominal spring constant 200 N/m) has a spherical tip with a nominal radius of 30 nm. The measurement consists of the following steps: first, the deflection sensitivity of the probe on a fused silica sample (Bruker) was determined; next, approach and retract force curves on the polymer brush samples were collected with an approach and retract velocity of 1 µm/s. The peak force setpoint and trigger threshold were adjusted to obtain a 2-10 nm indentation depth into the polymer brush samples. The deflection vs displacement raw data was converted to force vs distance curves using the method by Ducker et al.⁴⁹ To determine Young's modulus values of the polymer brush samples, the approach force distance curves were fitted to the Derjaguin-Muller-Toporov (DMT) model as shown in **Equation 1**.

$$F = Def.*k = \frac{4}{3} \frac{E}{1-v^2} R^{1/2} \delta^{3/2}$$
 (1)

In this equation, F is the force (nN) obtained from approach force distance curves, Def. is the deflection sensitivity, k is the spring constant (N/m) of the cantilever, E is the Young's modulus (GPa), ν is the Poisson ratio (0.3 was used), R is the tip radius (nm), and δ is the indentation depth (nm).

Synthesis

Synthetic procedures for the preparation of the monomers and initiators used in this study can be found in the Support Information.

Solution polymerization of benzyl protected para-OOB-AB-P or meta-OOB-P-AB monomers

A typical polymerization procedure utilizing the initiator DMA-P and the monomer of interest is depicted below in Scheme 1. Monomer (para-OOB-P-AB or meta-OOB-P-AB) (0.216 g, 0.5 mmol) and DMA-P (3.4 mg, 0.0125 mmol) were placed in a round bottom flask and then degassed three times with nitrogen, followed by the addition of THF (10 mL) via a degassed syringe. The flask was then placed in a methanol and water mixture cooled with dry ice to -20 °C for 10 min to cool. The 1 M lithium bis(trimethylsilyl)amide (LiHMDS) base in THF (0.6 mL, 0.6 mmol) was then rapidly injected and the solution stirred while aliquots were taken for kinetic studies or for 1 h for bulk polymers. For the kinetic studies, 2 mL aliquots were withdrawn using a degassed syringe at one min intervals. Aliquots and bulk polymerizations were immediately quenched with 5 mL saturated aqueous ammonium chloride after being withdraw with syringe or completing the desired polymerization time. The polymer was then isolated via extraction with DCM and dried over anhydrous magnesium sulfate. DCM was then removed at room temperature using a rotary evaporator before further drying the obtained polymer in a vacuum oven at 60 °C for 2 h.

Removal of protecting side chain of para- and meta-substituted polymers

To remove the protecting side chain from the synthesized polymers (**Scheme 1**), 0.1 g of polymer was dissolved in 2 mL of DCM. To this solution, 2 mL of trifluoroacetic acid (TFA) was added and the solution was stirred at room temperature for 72 h. After this time, the TFA and DCM were removed at 40 °C using a rotary evaporator. The polymer was then dispersed in DCM using sonication to dissolve the cleaved side chains. The insoluble polymer was then filtered off using

gravity filtration and rinsed with DCM. The obtained polymer was dried in a vacuum oven at 120 °C for 1 h before characterization using NMR and FTIR spectroscopy.

Preparation of 500 nm Stöber silica

Stöber silica was synthesized as previously reported.³⁰ Stöber silica particles, approximately 500 nm in diameter, were synthesized by adding 300 mL of absolute ethanol and aqueous ammonia (100 mL, 1.45 mol) into a 500 mL round bottom flask with a stir bar. Tetraethyl orthosilicate (TEOS) (25 mL, 112 mmol) was then added at room temperature while stirring vigorously. After 12 h, the particles were washed three times with anhydrous ethanol using sonication/centrifugation wash cycles. The particles were then dried in a vacuum oven and calcined in a tube furnace at 600 °C for 4 h open to air. The particles were subsequently hydrolyzed by heating the silica particles (5 g), 40 mL of 30% hydrogen peroxide solution, and 20 mL of ethanol to 75 °C for 24 h. The hydrolyzed particles were centrifuged and dried in vacuum oven at 60 °C for 2 h. The final particles were characterized using TEM and TGA.

Deposition of MDMS-Amide-P initiator on flat silica wafers

Silica wafers cut into 1x2 cm pieces were placed in a glass petri dish. Piranha solution (7 mL sulfuric acid and 3 mL 30% aqueous hydrogen peroxide) was poured into petri dish and set at 100 °C for 2 h and subsequently rinsed three times with DI water. Anhydrous toluene (10 mL) and MDMS-Amide-P (0.1 g, 0.25 mmol) were then added to a 10 mL reaction vial with the cleaned wafers, which was then capped with a glass stopper. The solution was heated to 100 °C for 2 h without stirring. The initiator-modified wafers were then sonicated with fresh toluene twice and THF once, to remove unreacted initiator, and finally annealed in an oven at 140 °C for 30 min. The final wafers were characterized using ellipsometry, goniometry, and GATR-FTIR spectroscopy.

Deposition of MDMS-Amide-P initiator on Stöber silica

3 g of Stöber silica was placed directly into a 500 mL round bottom reaction flask. Anhydrous toluene (350 mL) and MDMS-Amide-P (0.5 g, 1.2 mmol) were added to the flask, which was then capped with a glass stopper. The solution was heated to 100 °C for 2 h with stirring. After this time, the particles were washed with repeated centrifugation/suspension cycles, twice in toluene and once in THF, using centrifuge tubes. The resulting powder was dried in a vacuum oven at 60 °C for 1 h to give an off-white powder. The initiator-modified particles were characterized using TEM and TGA.

Formation of polymer brushes on flat silicon wafers

MDMS-Amide-P modified wafers were placed into a 25 mL round bottom flask along with a stir bar and the desired monomer (para-OOB-P-AB or meta-OOB-P-AB) (0.108 g, 0.25 mmol), and the flask was then sealed with a rubber septum. The flask was placed under vacuum for 1 h before being degassed and backfilled with nitrogen three times. After this, dry THF (3 mL) was added to the flask using a degassed syringe. The flask was then placed in a methanol and water mixture cooled with dry ice and allowed to cool for 10 min at -20 °C. LiHDMS (0.3 mmol, 0.3 mL) was then rapidly added using a degassed syringe to start the polymerization. The polymerization was allowed to proceed at -20 °C for 1 h. After this time, the flask was unsealed, and the wafers removed. The polymer formed in solution was then quenched with 5 mL saturated aqueous ammonium chloride solution and isolated via extraction with DCM, before being dried over anhydrous magnesium sulfate. DCM was then removed at room temperature using a rotary evaporator before further drying in a vacuum oven at 60 °C for 2 h. The polymer-modified wafers were cleaned via sequential sonication in THF, chloroform twice, and THF again, before being finally dried under a stream of nitrogen. The polymer-modified wafers were characterized using

ellipsometry, goniometry, GATR-FTIR spectroscopy, and AFM. Polymer formed in solution was characterized using NMR and GPC.

Formation of polymer brushes on Stöber silica

MDMS-Amide-P modified Stöber silica (0.5 g) was placed into a 25 mL round bottom flask along with a stir bar and the desired monomer (para-OOB-P-AB or meta-OOB-P-AB) (0.432 g, 1 mmol), and the flask was then sealed with a rubber septum. The flask was placed under vacuum for 1 h before being degassed and backfilled with nitrogen three times. After this, dry THF (10 mL) was added to the flask using a degassed syringe. The flask was then placed in a methanol and water mixture cooled with dry ice and allowed to cool for 10 min at -20 °C. LiHDMS (1.2 mmol, 1.2 mL) was then rapidly added via a degassed syringe to start the polymerization. The polymerization proceeded for 1 h before being quenched with 5 mL of a saturated aqueous ammonium chloride solution. The polymer-modified Stöber silica was isolated and cleaned by repeated centrifugations and washings with THF, chloroform twice, and THF using plastic centrifuge tubes and sonication. The final polymer-modified particles were then dried in vacuum oven at 60 °C overnight before characterization with TGA and TEM.

Removal of the protecting side chain of para- and meta-substituted polymers on modified wafers. To remove the benzyl protecting side chain from the polymer brushes on the silicon wafers, a polymer-modified wafer was placed in a round bottom flask containing 2 mL of DCM. The flask was sonicated for 10 min, followed by the addition of 2 mL of TFA. The flask was then stirred for 72 h at room temperature. After this time, the wafer was removed from the flask, placed in 10 mL of THF, and sonicated for 10 min. The wafer was finally heated in dimethylacetamide (DMAc) to remove any remaining physically absorbed material. The cleaned wafers were then dried in a

vacuum oven at 60 °C for 1 h and characterized using ellipsometry, goniometry, GATR-FTIR spectroscopy, and AFM.

Removal of protecting side chain of para- and meta-substituted polymers on modified silica particles

To remove the benzyl protecting side chain from the polymer brushes on the Stöber silica, 1 g of polymer-modified Stöber silica was placed in a round bottom flask and sonicated in 10 mL of DCM until dispersed. 2 mL of TFA was then added to the dispersed Stöber silica solution and stirred for 72 h at room temperature. After this time, the TFA and DCM were removed at 40 °C using a rotary evaporator. The polymer-modified Stöber silica was then dispersed in THF using sonication for 10 min and centrifuged. Particles were then dispersed in DMAc and heated to 100 °C for 10 minutes before cooling to room temperature and centrifuging. The polymer-modified Stöber silica was then dried in vacuo at 60 °C for 1 h and characterized using TGA and TEM.

Results and Discussion

Aromatic polyamides are classified as high-performance polymers due to their outstanding mechanical properties and exceptional thermal resistance, which arise from their rigid aromatic amide linkages and hydrogen bonding between the chains. However, these also result in solubility problems and make producing well-defined polymers difficult, both of which inhibit the use of these materials for new applications and limit optimization of current applications. One such area is the preparation of aromatic polyamide coatings. While aromatic polyamides have been used as coatings for RO and gas separation membranes, the lack of covalent attachment and the difficulty in controlling the properties of the polymers using the current synthetic methods has inhibited the further development of these membranes and the expansion of these materials to new areas.

Recently, we reported on the use of substituent effect CGC polymerization for the preparation of aromatic polyamide brushes.³⁰ The adaptation of this synthetic technique to a surface-initiated polymerization allowed for the synthesis of covalently attached, well-defined aromatic polyamide coatings. The success of this technique is dependent on the ability to convert the traditional stepgrowth polymerization used for aromatic polyamides to a chain-growth process. A limitation of our previous work was the use of an octyl side chain, on the nitrogen of the amide linkage, to improve solubility of the polymer. The presence of this side chain eliminates the strong hydrogen bonding, which is characteristic in most commercial aromatic polyamides. To produce aromatic polyamide brushes with the exceptional properties observed in the conventional polymers, we have hypothesized that the protection-deprotection process used in solution by Yokozawa could be adapted to our surface-initiated system.^{34,35,46,50,51}

Monomer and Initiator Synthesis

Similar synthetic routes to Yokozawa and our earlier work were utilized to produce each monomer and both solution and surface initiators.^{30,44,45} Para- and meta-substituted monomers were synthesized using the same procedure starting with either 4- or 3-nitrobenzoyl chloride, respectively. In short, the nitrobenzoyl chloride was reacted with phenol to introduce the desired leaving group for these monomers. Then the nitro groups were reduced using palladium on carbon in ethyl acetate under a hydrogen atmosphere. Once reduced, the protecting group was added to the amine via reaction with 4-octyloxybenzaldehyde using reductive amination. Both monomers were synthesized in reasonable yields and high purity.

A new initiator was synthesized for the substituent effect CGC surface polymerizations in order to produce well defined polymers (**Scheme 1**). The same solution initiator that was used in our previous solution studies was utilized in this study.^{44,45} The new surface initiator incorporated the

same ester leaving group and electron withdrawing amide as the solution initiator but was improved upon from our initial surface studies by reducing the number of methoxy silane groups on the attachment group from three to two. This has been previously shown to lower the tendency towards side condensation reactions and produce more uniform surfaces.⁵² The silane surface initiator was synthesized by reacting phenyl 4-(chlorocarbonyl)benzoate with N-methylaminopropylmethyldimethoxysilane and was produced with good yield and high purity.

Scheme 1. Synthetic strategy for the preparation of meta- (A) and para- (B) substituted aromatic polyamides with a protecting side chain in solution and the subsequent deprotection process.

Solution Polymerizations of the Protected Monomers

Yokozawa has performed similar solution polymerizations of both meta- and para-substituted benzyl ether monomers, demonstrating that aromatic polyamides containing the benzyl ether leaving group could be produced in a controlled manner leading to polymers with low PDI's and well-defined molecular weights.⁴³ However, detailed kinetic studies were not reported in these studies. Obtaining a thorough understanding of the kinetics for the different monomers is important in adapting their solution polymerization to a surface-initiated system. As such, the solution kinetics for both the meta- and para-substituted monomers containing the benzyl ether side chain were examined. From the semi-logarithmic plot of conversion versus time (Figure 1), both the meta- and para-substituted protected monomers exhibit first order kinetics, which is indicative of maintaining an active number of reactive chains throughout the polymerization. From these studies, it was determined that the rate constant of propagation (k_p) for the meta-substituted protected monomer was 3.92 M⁻¹s⁻¹, which was nearly threefold that of the para-substituted protected monomer at 1.38 M⁻¹s⁻¹. This was hypothesized to be due to the para-substituted protected system exhibiting a stronger deactivation of the carbonyl of the ester in the substituent effect GCG polymerization via resonance, compared to inductive effect observed with the metasubstituted protected system, for both monomer and growing polymer chain. However, both

systems had a larger kp 2 when compared to the 1.8 1.6 previously studied para 1.4 $k_p = 3.92 \text{ M}^{-1}\text{s}^{-1}$ octyl monomer, which 1.2 1 had a k_p of 0.64 $M^{-1}s^{-1}$ 0.8 0.6 1 44 0.4 During $k_p = 1.38 \text{ M}^{-1}\text{s}^{-1}$ the kinetic 0.2 0 studies, it was 300 0 100 200 400 500 600 Time (seconds) observed, as expected,

that the transparency of the polymerization solution for the

Figure 1. Semi-logarithmic plot of conversion versus time for the solution polymerization of meta- (red) and para- (blue) substituted protected monomers.

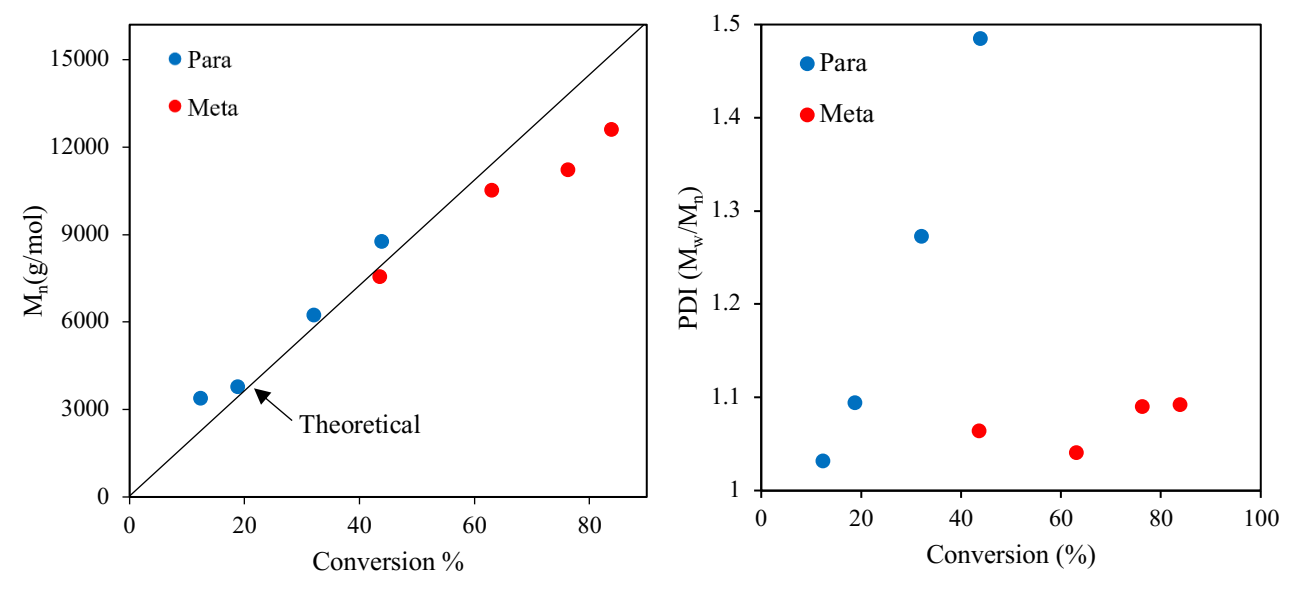
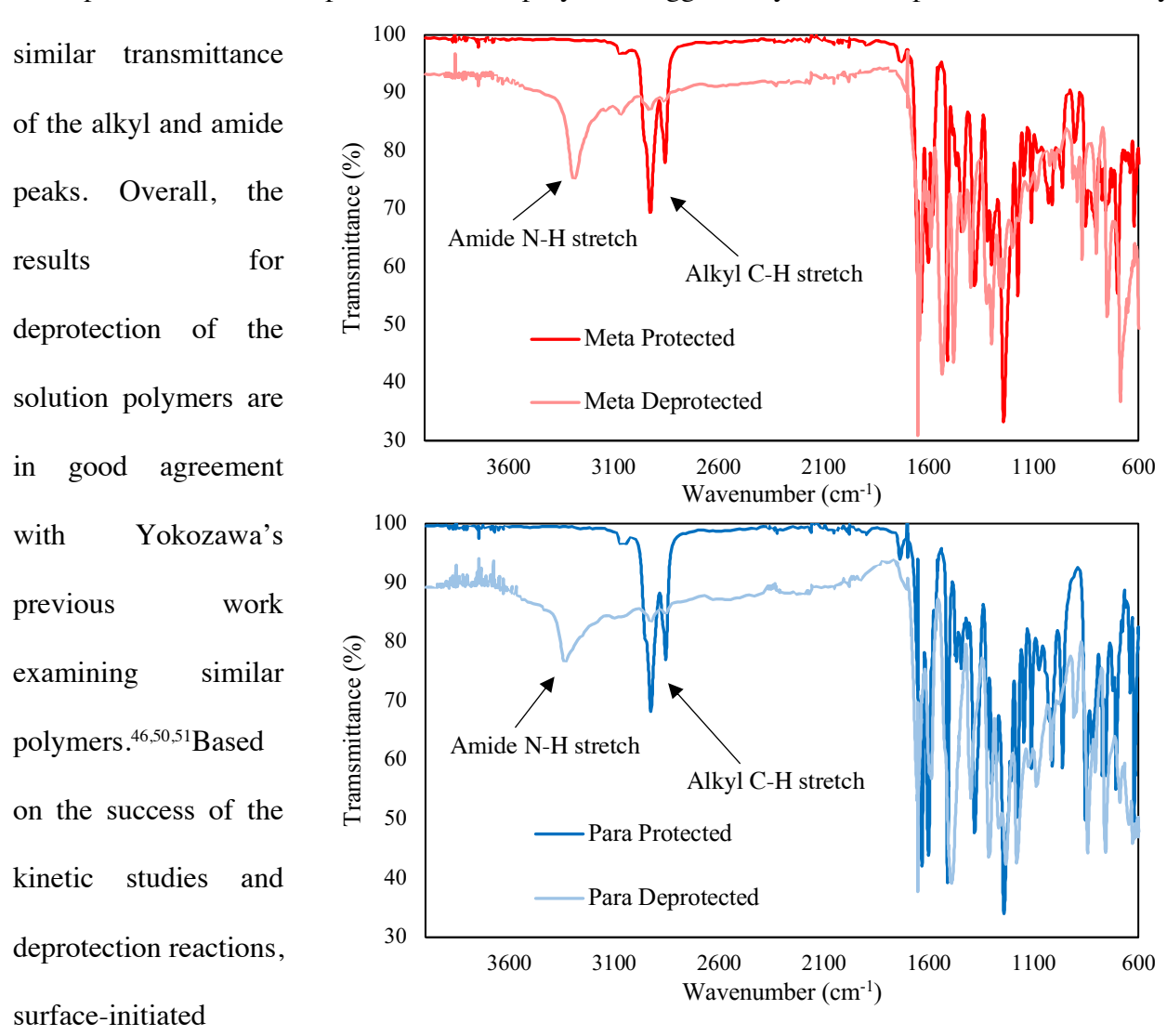


Figure 2. Plots of number average molecular weight (M_n) (left) and PDI (right) versus monomer conversion for the solution polymerization of meta- (red) and para- (blue) substituted protected monomers.

meta-substituted aromatic polyamide with the protecting side chain was greater than the parasubstituted system. In the case of the para-substituted polymer, the polymerization solution remained clear until an estimated degree of polymerization (DP) of 12, which corresponded to a molecular weight of approximately 4000 g/mol, after which it became opaque. This change in solution properties was also observed in the solution kinetics examining molecular weight and PDI versus monomer conversion (Figure 2). In these plots, between a M_n of 3800 g/mol and 6260 g/mol for the para-substituted monomer, the PDI shows an increase from 1.09 to 1.27 and continues increasing to 1.5 at a M_n of 8800 g/mol. Comparing this to the meta-substituted polymer, the PDI remains low, typically less than 1.1, throughout the polymerization and the polymer remained soluble in THF, as evidenced by the transparent polymerization solution. It is hypothesized that the change in solution properties for polymerization of the para-substituted monomer is due to chain aggregation in solution rather than precipitation of the polymer. This conclusion was reached as there was no settling of precipitate over time if stirring of solution was stopped and the molecular weight of the polymer continued to grow even after the solution became opaque, as evidenced by a monomodal peak in the GPC analysis. Due to this potential chain aggregation of the para-substituted polymer at higher molecular weights in THF, chloroform was used as the GPC solvent to allow molecular weight characterization of these samples without interference to the light scattering detectors. However, chloroform cannot be used as the polymerization solvent due to the strong base, LiHDMS, used in the polymerization system, as this would deprotonate the chloroform. Despite the differences in solution properties, Figure 2 demonstrates approximately linear growth of polymer molecular weight with conversion for both monomers. This is indicative of a controlled chain-growth polymerization with a constant number of polymer chains and fast initiation relative to propagation, which are both characteristics required for the formation of uniform polymer brushes.⁵³

Deprotection of the Aromatic Polyamides Produced in Solution

Yokozawa has previously demonstrated deprotection of both the meta- and para-substituted benzyl ether protected polymers using either pure TFA or TFA in DCM. 34,35,50,51 Using this work as a starting point, both the meta- and para-substituted benzyl ether protected polymers were placed in a TFA/DCM solution for 72 h (Scheme 1). During the deprotection reaction, the para-substituted polymers formed an off-white precipitate that was insoluble in chloroform, DCM, dimethyl sulfoxide (DMSO), and THF. As such, only FTIR spectroscopy characterization was performed for these deprotected polymers (Figure 3). The meta-substituted polymers also formed an offwhite precipitate during the reaction that was insoluble in chloroform and DCM. However, the meta-substituted deprotected polymers were soluble in DMSO, allowing for both FTIR (Figure 3) and NMR spectroscopy characterization (Figure S1). Comparing the benzyl ether protected and deprotected meta-substituted polymers using NMR, a peak at 10.6 ppm appeared after the deprotection reaction, showing the presence of an N-H amide proton, and the peak for the benzylic proton at 4.8 ppm almost completely disappeared, confirming the successful deprotection of the polymer (Figure S1). To determine the efficiency of the reaction, the aromatic peaks at 8.38 ppm were integrated and compared to the integrated alkyl methyl end group peaks of the protecting side chain at 0.81 ppm, which indicated 94% deprotection efficiency for the meta-substituted polymer. FTIR spectroscopy demonstrated that both the deprotected meta- and para-substituted polymers had a broad amide proton stretch at approximately 3300 cm⁻¹, when compared to the protected versions of the polymer, and the alkyl C-H stretches from the protecting benzyl ether side chain at 2920 and 2850 cm⁻¹ had also mostly disappeared (**Figure 3**). Comparison of the FTIR spectra for the deprotected meta- and para-substituted polymers suggest very similar deprotection due to very



polymerizations of the meta- and parasubstituted monomers were next performed

Figure 3. FTIR spectra comparing the protected and deprotected aromatic polyamides for both the para- (bottom) and meta- (top) substituted solution polymers.

on both flat and high surface area silica surfaces.

Synthesis and Deposition of Silane Based CGC Initiator (MDMS-Amide-P)

A similar silane CGC initiator to our previous work was synthesized for this study (**Scheme 2**).³⁰ The initiator in this work was designed to incorporate two improved functionalities compared to the previous surface-based initiator. As mentioned previously, the first change was the functionality on the silane attachment group of the initiator. In this case, two hydrolysable methoxy groups were used in place of the three in the original initiator. This allows for less branching and crosslinking of the silane in solution and leads to a more uniform film on the surface.^{54,55} The second aspect of the initiator that was improved was the leaving group of the ester. For the initiator used in this study, the leaving group of the ester was changed to a phenyl ester moiety, instead of the previous methyl ester, as it is similar to the solution initiator, has been shown to provide better control over the polymerization, and the lithium phenoxide produced as a by-product of the initiation process demonstrates excellent solubility in the THF reaction media.^{44,45}

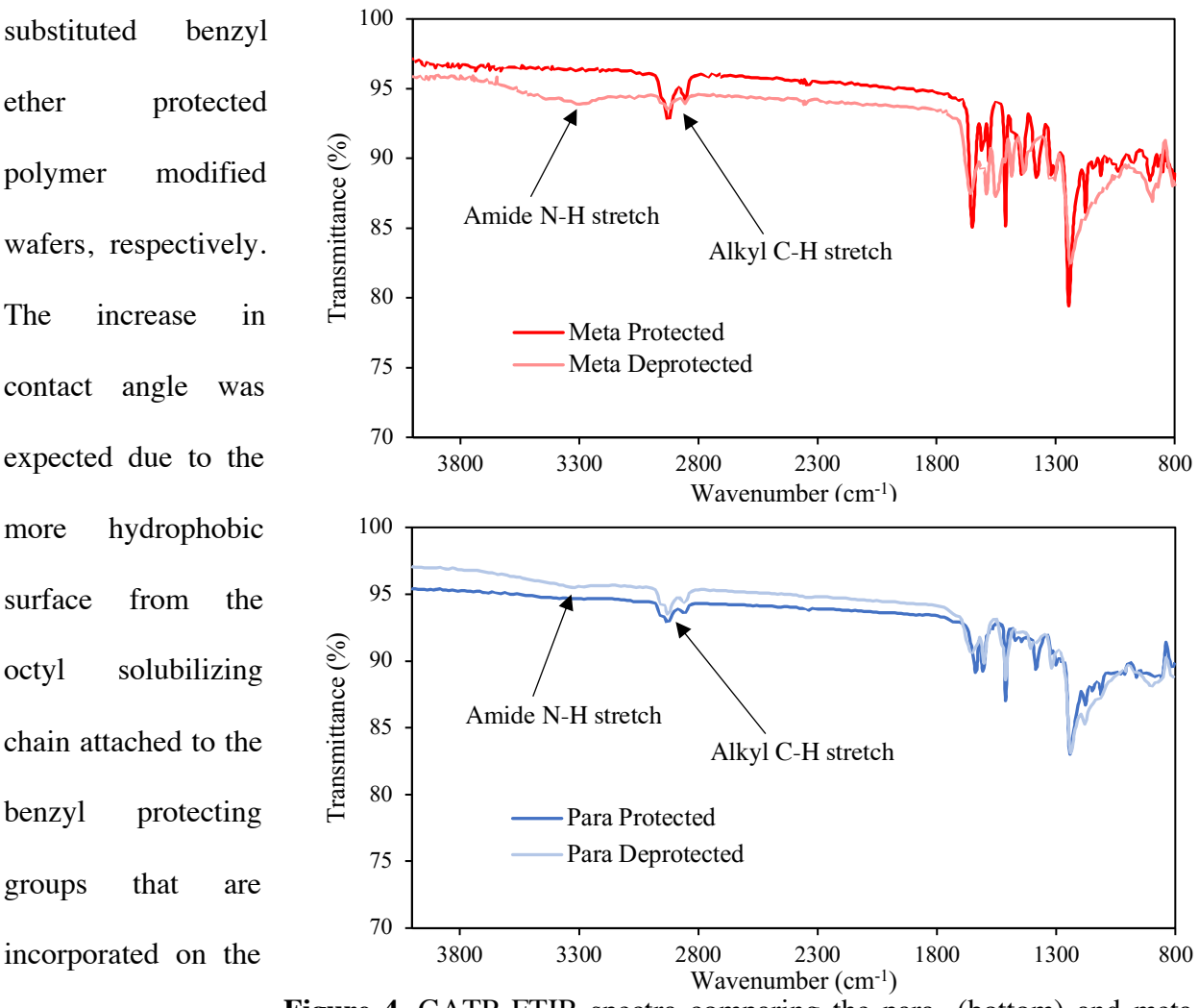
The new initiator for the surface-based CGC polymerizations, MDMS-Amide-P, was deposited on piranha-cleaned flat silicon wafers in anhydrous toluene at 100 °C for 2 h, followed by sonication with fresh toluene twice and THF once to remove unreacted initiator. The initiator-modified wafers were blown dry between sonication washes before finally being annealing in a vacuum oven at $140 \,^{\circ}$ C for 30 min. Goniometry analysis of the wafers before and after surface modification with the initiator showed an increase in water contact angle from a surface that is essentially completely wetted (~5-10°) for the clean wafers to a contact angle of $74 \pm 1.7^{\circ}$ for the wafers with the deposited MDMS-Amide-P initiator. These results are consistent with a change from the initial hydroxylated silicon surface to the more hydrophobic phenyl ester terminal moiety. Ellipsometry measurements show that the thickness of the film increases from the initial silica layer thickness of $2.3 \pm 0.1 \,^{\circ}$ nm to a thickness $3.0 \pm 0.6 \,^{\circ}$ nm, using the same SiO₂ model to fit the data, after deposition of the initiator. The low error in the measurements suggests a good model fit to the

ellipsometry data and a uniform MDMS-Amide-P initiator film. GATR-FTIR spectroscopy performed on the deposited MDMS-Amide-P film on silicon wafers showed similar peaks to the previous methyl ester study (**Figure S2**).³⁰ Pertinent absorption bands indicative of the MDMS-Amide-P molecule are evident with peaks at approximately 2850 and 2930 cm⁻¹, corresponding to the alkane C-H stretches, along with peaks at 1730 cm⁻¹, for the carbonyl stretch of the ester leaving group, and 1650 cm⁻¹, corresponding to the amide carbonyl stretch. The peaks at 1200 cm⁻¹ and 900-800 cm⁻¹ are present in a spectrum for clean, unmodified silicon wafers and can be assigned to the Si-O-Si stretch and Si-O-H stretch & bend modes for silica, respectively.⁵⁶

Growth of Aromatic Polyamide Brushes from Surface-Immobilized Initiators on Flat Silicon Substrates Employing the Benzyl Protected Monomers

To determine the effectiveness of the surface-immobilized MDMS-Amide-P initiator for CGC polymerization, aromatic polyamide brushes were grown by immersing the initiator-modified silica wafers in a solution of deprotonated monomer, either the meta- or para-substituted benzyl ether protected, in THF at -20 °C (Scheme 2). After the polymerization, the polymer-modified wafers were extensively cleaned using sonication to remove unreacted monomer and physically absorbed self-initiated polymer to ensure characterization was focused on the surface-immobilized polymer. Like the previously discussed solution polymerizations, both the meta- and para-substituted benzyl ether protected monomers were used for the preparation of polymer brushes. It was once again observed that during polymerization of the para-substituted benzyl ether protected monomer the solution turned opaque over time, which was attributed to self-initiation of monomers in solution and the chain aggregation of the polymer at higher molecular weights, as previously discussed. Whereas the meta-substituted benzyl ether protected polymer solutions

remained clear throughout the polymerization, although NMR analysis of the polymerization solution indicated that self-initiation was still observed, resulting in polymer forming in solution. Goniometry measurements demonstrated that the water contact angle of the modified wafers increased from $74\pm2^{\circ}$ for the immobilized initiator to $94\pm2^{\circ}$ and $95\pm2^{\circ}$ for the meta- and para-



surface as part of the Figure 4. GATR-FTIR spectra comparing the para- (bottom) and meta-repeating unit for (top) substituted protected and deprotected aromatic polyamide brushes on both polymer chains.

The thicknesses of

the polymer films were measured using ellipsometry. To find the best fit for determining the

thickness, a Cauchy model was used.⁵⁷ The use of the Cauchy model was justified based on the wavelength range of 465 to 635 nm for the ellipsometer, where the polymer films are nonabsorbing. In addition, the Cauchy model allowed for a more appropriate fit of the data to the model with an extracted index of refraction for the aromatic polyamide brush films being 1.56, instead of using silica's index of refraction of 1.45. From this thickness analysis, it was determined that the thickness of the aromatic polyamide brushes created using the system developed in this study were almost five times thicker than films achieved using the methyl ester method in our first report on the octyl substituted monomer. 30 Thicknesses of up to 57 ± 4 nm were obtained for the para-substituted protected aromatic polyamide brushes, whereas the meta-substituted protected brushes achieved thickness up to 46 ± 1 nm. GATR-FTIR spectroscopy (Figure 4) shows, as expected, that the surface-immobilized polymers had near perfect spectral overlap when compared to those of the same polymers prepared in solution (Figure 3). Using AFM, the topography of both para- and meta-substituted benzyl ether protected surfaces were examined (Figure 5). The AFM analysis showed a low root-mean-square (rms) roughness for both surfaces, with the metasubstituted protected polymer surface having a rms of 1.04 ± 0.19 nm and the para-substituted system had a rms of 2.29 ± 0.29 nm. The higher rms value for the para-substituted benzyl ether protected polymer is possibly due to some aggregation of the chains due to the more linear backbone. The AFM image for this surface does indeed show the presence of small features on the surface that are consistent with chain aggregation. The AFM low rms roughness values for both surfaces suggest excellent control was achieved during the surface-initiated polymerization, resulting in well-defined polymer films.

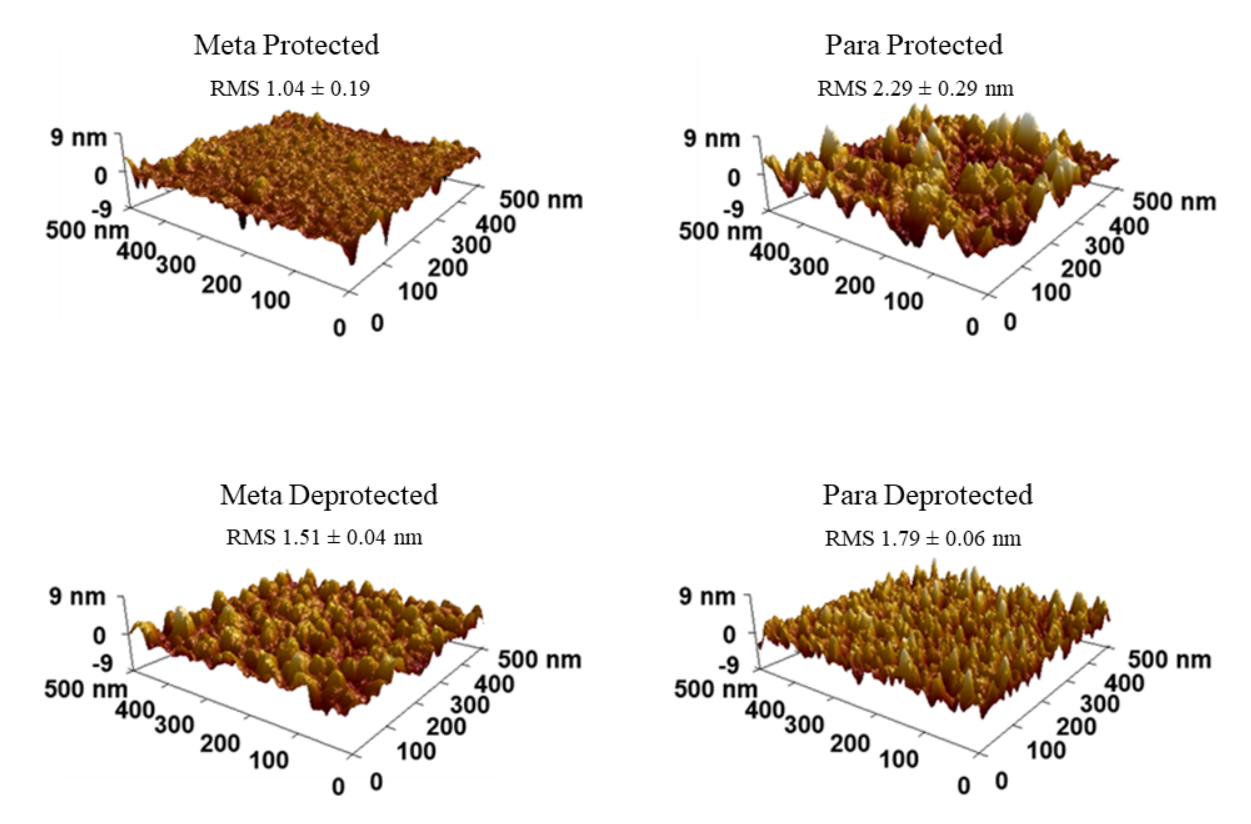


Figure 5. AFM 3D images with a scan size of 500 nm for meta protected, meta deprotected, para protected, and para deprotected surface profiles.

Scheme 2. Substituent effect CGC polymerization for the preparation of a meta-substituted benzyl ether protected polymer brush and the subsequent deprotection reaction on flat or curved silica surfaces. The same procedure was used for the para-substituted monomer.

Deprotection of Polyamide Brushes on Silica Wafers

Following a similar strategy to the solution polymers, the protected aromatic polyamide brushes were deprotected by placing them in a solution of TFA and DCM for 72 h (**Scheme 2**). After this time, the brushes were sonicated in THF and heated in DMAc to remove any physically absorbed benzyl ether side chains from the surface. The deprotected polymer brushes were characterized using GATR-FTIR spectroscopy, ellipsometry, goniometry, and AFM. Goniometry showed the water contact angle decreased from $94 \pm 2^{\circ}$ to $81 \pm 2^{\circ}$ after the deprotection reaction for the metasubstituted polymer brushes and from $95 \pm 2^{\circ}$ to $81 \pm 2^{\circ}$ for para-substituted brushes. This is hypothesized to be due to the removal of the hydrophobic octyl solubilizing chain off the benzyl

ether protecting group. Ellipsometry showed a decrease in the thickness of the brushes after the deprotection reaction, which was expected, due to loss of the protecting side chain that comprised approximately 65 wt.% of the polymer repeating unit.⁵⁸ It is also possible that hydrogen bonding between the amide proton, present after the deprotection reaction, and the amide carbonyl groups on the polymers contributes to the observed thickness decrease due to the polymer chains forming aggregates on the surface. The meta-substituted aromatic polyamide brushes exhibited a decrease in thickness from 46 ± 1 nm to 23 ± 1 nm, while the para-substituted brushes had a decrease from 57 ± 4 nm to 21 ± 2 nm. The larger decrease in thickness for the para-substituted brush after the deprotection reaction may be due to the reduced solubility of the deprotected para-substituted brush in dichloromethane. As the deprotection reaction progresses, the para-substituted brush will precipitate out of solution, which would result in a larger decrease in the observed thickness compared to the meta-substituted polymer that is more soluble in dichloromethane.

Removal of the protecting benzyl ether side chain was also characterized using GATR-FTIR spectroscopy (**Figure 4**). In both cases, comparison of the spectra before and after the deprotection reaction showed the reduction of alkyl side chains the C-H stretches near 2850 and 2930 cm⁻¹ and the appearance of a small amide proton peak at 3300 cm⁻¹. However, the spectra for the deprotected para-substituted polymer brush (**Figure 4**) still shows significant C-H stretches, which suggest the deprotection reaction was not as efficient for this system. We hypothesize the reason for this is the reduced solubility of the deprotected para-substituted polymer, compared to the deprotected meta-substituted polymer in the solvent used for the deprotection reaction, dichloromethane. As the deprotection reaction starts, the solubility of the para-substituted polymer brush will decrease, inhibiting removal of all the protecting groups. Whereas the meta-substituted polymer brush is more soluble and shows a larger decrease in the C-H stretches, indicating more efficient

deprotection. Despite the differences in deprotection efficiency, overall, the para-substituted polymer brush shows the largest decrease in thickness after deprotection due to the dominant solubility effect resulting in precipitation of the polymer brush from solution as the deprotection reaction occurs. Comparing the AFM topography of protected and deprotected surfaces, very similar rms roughness values were observed for both meta- and para-substituted surfaces (**Figure 5**). Despite the similar rms values, the AFM images show significant differences in the topographies of both the meta- and para-substituted surfaces after the deprotection reaction. The meta-substituted surface shows a slight increase in the RMS roughness and the presence of more pronounced surface features after deprotection (**Figure 5**). This is attributed to aggregation of the chains on the surface as a result of intermolecular hydrogen bonding. While the para-substituted surface had a decrease in the rms roughness after the deprotection reaction, the surface topography appears to be come more uniform and resembles that of the deprotected meta-substituted surface (**Figure 5**). Once again, we propose that this is due to intermolecular hydrogen bonding.

Growth of Aromatic Polyamide Brushes from Surface-Immobilized Initiators on High Surface

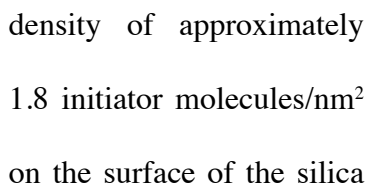
Area Silica Using Benzyl Protected Monomers

To gain greater insight to the properties of the surface-initiated aromatic polyamide brushes, Stöber silica particles were also used to prepare the same polymer brushes systems that were synthesized on flat silicon wafers. To achieve this, large Stöber silica particles (approximately 500 nm in diameter) were synthesized, calcined, rehydrated, and dried using a similar previously reported technique.⁵⁹ The large diameter particles were chosen as it has been reported they mimic the properties of flat silicon wafers and allow for effective comparison between the two different substrates.⁶⁰ The surface initiator was deposited on the Stöber silica by stirring the particles in hot anhydrous toluene with the MDMS-Amide-P initiator. The aromatic polyamide brushes then were

grown from the cleaned and dried initiator-modified particles using a similar procedure to that of the flat silicon wafers (**Scheme 2**). As was the case for the flat silicon wafers, the Stöber silica solution for polymerization of the para-substituted benzyl ether protected monomer became opaque, because of self-initiated polymer forming and aggregating in solution, while the solution for the meta-substituted monomer stayed transparent. After polymerization, the polymer-modified silica particles were isolated by extensive washings and centrifugations, and then dried and characterized using TEM and TGA.

TGA results for the aromatic polyamide polymer brushes prepared on the Stöber silica particles can be seen in **Figure 6**. TGA analysis of surface-initiated polymers is important, as it allows for the determination of the grafting density of the polymer chains and, thus, determination if a

polymer brush structure was synthesized. The TGA trace for MDMS-Amide-P initiator modified Stöber silica particles has an approximately 0.5 wt.% weight loss, when compared to the calcined silica. This weight loss corresponds to a grafting



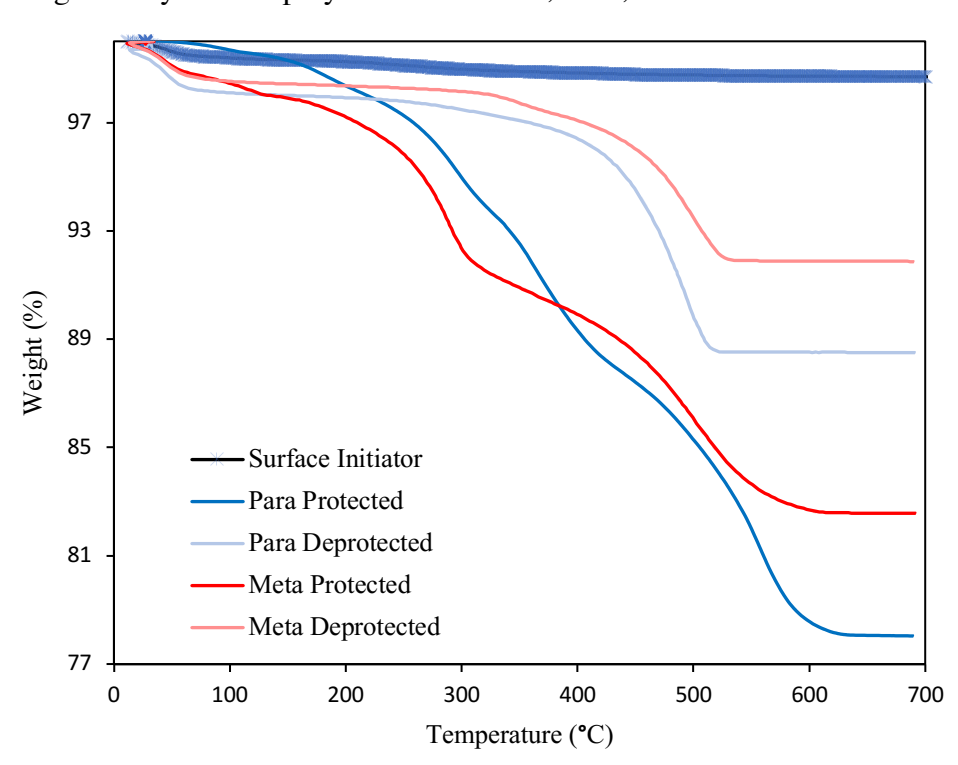


Figure 6. TGA profiles of the MDMS-Amide-P surface initiator (black) and meta- (red) and para- (blue) substituted protected and deprotected aromatic polyamide brushes on Stöber silica particles.

particles. This calculation was performed by using the wt.% of initiator lost in TGA, the molecular weight of the organic component of the MDMS-Amide-P initiator, and the surface area of the 500 nm spherical Stöber silica particles. When comparing these results to those previously reported, the initiator density for the MDMS-Amide-P system is approximately half of that observed for the methyl ester initiator.³⁰ This can be explained by the difference in the structure of the silane attaching group between the two initiators. As discussed previously, the MDMS-Amide-P initiator was designed with two hydrolysable methoxy groups on the silane compared to the three groups of the previously reported initiator to reduce condensation side reactions.⁵² Silanes with three hydrolysable groups have been shown to form crosslinked structures on the surface, which produces a higher number of groups per unit surface area but produces less uniform films.⁵⁵ When comparing weight loss of both polymers on the high surface area particles, the parasubstituted protected polymer demonstrates a higher weight loss, 20 wt.%, compared to the weight loss of the meta-substituted protected polymer, 15 wt.% (Figure 6). This was due to the thicker films produced with the para-substituted protected polymer, as discussed below. Despite this weight loss difference, both degradation profiles were very similar, with the para-substituted protected polymer degrading at a slightly higher temperature than the meta-substituted protected polymer. Onset degradation temperatures of 260 °C and 515 °C were found for the two degradation stages of the para-substituted protected polymer and 247 °C and 451°C for the meta-substituted protected polymer. The first derivative maximums were also used to find the weight loss slope maximums and gave 294 °C and 557 °C for the two degradation stages of the para-substituted protected polymer and 289 °C and 509 °C for the meta-substituted protected polymer degradation stages. The first stage of both degradation profile temperatures is very close and is hypothesized to be due to loss of the benzyl ether protecting side chain. This side chain corresponds to

approximately 65% of the weight of the polymer repeat unit. However, both polymers only showed an approximately 52% weight loss in this stage, which does not account for all the protecting side chains. The second burn off stage at higher temperature is hypothesized to correspond to degradation of the polymer backbone. The second stage of degradation for both polymers is comparable to similar aromatic polyamide structures, such as Kevlar® and Nomex® fibers, and corresponds closely to their degradation temperatures. ⁶¹ They also are very close to the degradation profiles for the meta- and para-substituted deprotected polymers, which will be discussed below. To further examine the protected brushes, grafting densities of both polymer brushes were obtained and compared to our previous study.³⁰ To do this, the polymers must be degrafted from the Stöber silica particles and their molecular weight properties determined. To degraft the polymer brushes, the particles were first suspended in THF, hydrofluoric acid (HF) added, and the suspension was stirred at room temperature for 1 h. The cleaved polymers were then extracted and characterized using NMR spectroscopy, GPC, and FTIR spectroscopy. NMR of the degrafted polymer showed the same proton peaks observed in the spectra of similar solution polymers (Figure S3). GPC gave a M_n of 97,240 g/mol with a PDI of 1.09 for the meta-substituted protected polymer and a M_n of 122,900 g/mol and PDI of 1.38 for para-substituted protected polymer. This demonstrates that the meta-substituted polymerization remained controlled throughout, while the para-substituted polymerization resulted in an increased PDI because of chain aggregation, as discussed above, which follows what was observed in the solution kinetic studies. It should be noted that, while the molecular weights prepared in the solution kinetic studies were much small than those obtained for the surface-initiated systems, a lower concentration of initiator is present on the surface of the particles when compared to that used in the solutions studies. Solutions polymerization were conducted for both the meta- and para-substituted protected monomers with an initiator

concentration of 0.002 mmol/L or targeting a theoretical DP of 500 to mimic the lower initiator concentration present on the surface and in each case the M_n values were greater than 80,000 g/mol and similar PDI's were observed. FTIR for both meta- and para-substituted protected polymers showed the same characteristic peaks that were seen in the solution polymers (Figure S4). Using the TGA weight loss percent of the particles along with the observed M_n, grafting densities of 0.30 chains/nm² for the meta-substituted protected polymer and 0.28 chains/nm² for the para-substituted protected polymer were calculated, using the same process as used in our previous work.³⁰ Comparing to our previous study, these grafting densities are similar and show that both the metaand para-substituted systems are within the reported polymer brush regime, indicating that a high level of chain packing on the surface was obtained for these polymer brush surfaces.¹⁰ Using TEM, the protected aromatic polyamide brush thicknesses were measured to be 22 ± 4 nm and 18 ± 3 nm for the para- and meta-substituted protected polymer brushes, respectively, and appeared to be very uniform across the surface of both particles (Figure 7). The lower thickness of the aromatic polyamide brush on the Stöber silica particles, compared to the silicon wafers, is attributed to the higher concentration of initiators on the silica particles relative to the amount of monomer present in the reaction mixture, when compared to the flat wafers. The silicon wafers have roughly 6 orders of magnitude less initiator molecules present in the reaction, so these initiators would see more monomer over the course of the reaction when compared to the Stöber silica particles. As the polymer molecular weight, which is proportional to the thickness of the polymer brushes, is a function of the ratio of monomer concentration to initiator concentration, the polymer on the flat wafers should have a higher molecular weight and, hence, brush thickness, which is indeed the case. As mentioned previously, the thickness of the polymer layer on the particles is very uniform for both the meta- and para-substituted protected polymers, suggesting a

well-defined polymerization process was obtained. When compared to the results for the methyl ester system in our previous work, where no obvious polymer was observed, the aromatic polyamide brushes produced from the phenyl ester monomer proved to be much thicker on both the silicon wafer and high surface area particles.³⁰

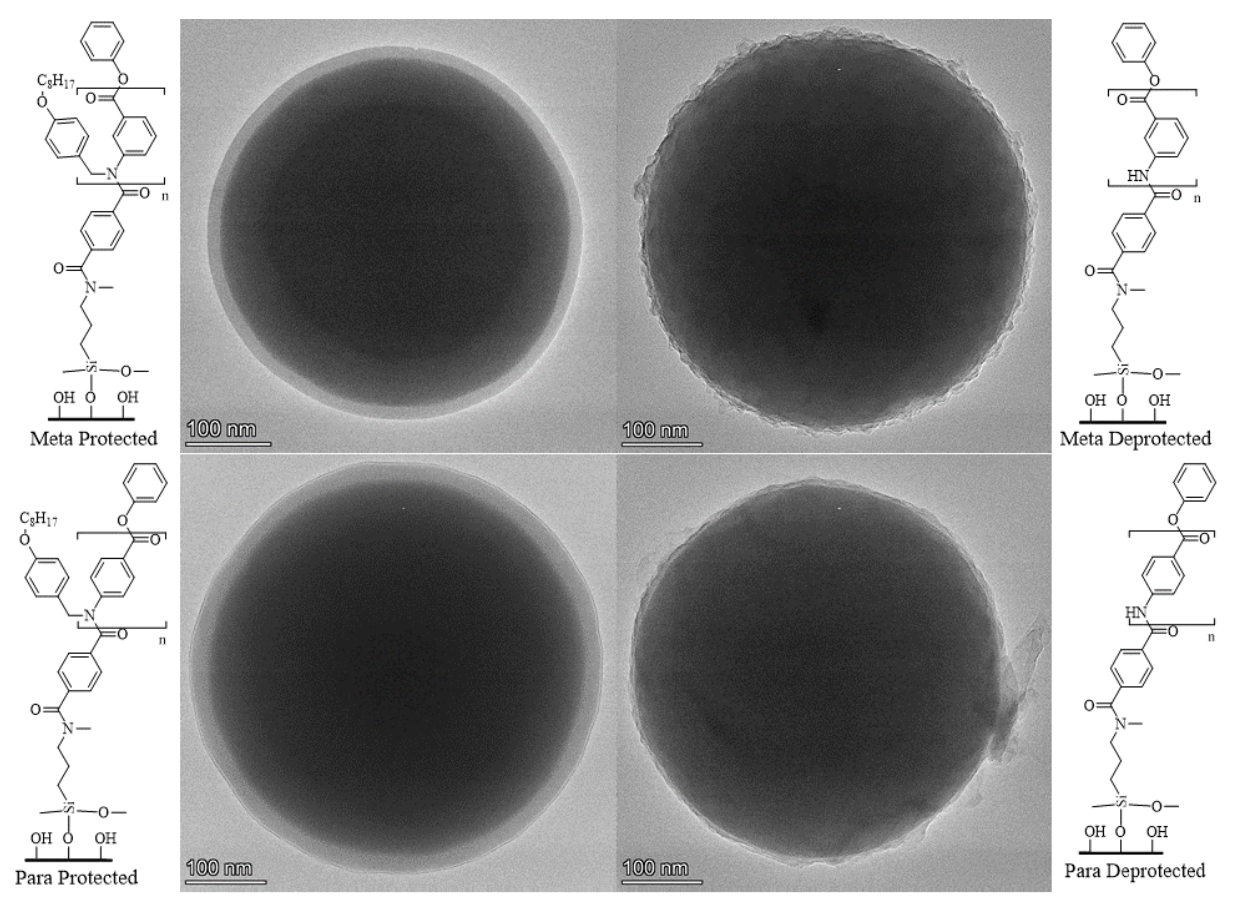


Figure 7. TEM images of hybrid Stöber silica particles with meta- (top) and para- (bottom) substituted protected polymer brushes (left) and deprotected polymer brushes (right).

Deprotection of Polyamide Brushes on High Surface Area Silica

To further investigate the aromatic polyamide brushes prepared on Stöber silica, the polymers were deprotected using a similar process as the flat silicon wafers. The particles were first suspended in DCM, followed by the addition of TFA, and were then stirred for 72 h. The particles were then

thoroughly cleaned with chloroform and heated in DMAc to remove physically absorbed side chains. The deprotected meta- and para-substituted polymer brushes on the Stöber silica were then characterized using TGA. These results showed a decreased weight loss for both meta- and parasubstituted deprotected brushes but did not get to the calculated 65 wt.% repeat unit mass loss expected with the removed side chain. Instead, a 54 wt.% decrease was observed for the parasubstituted deprotected polymer brushes and 55 wt.% for the meta-substituted deprotected polymer brushes when compared to the protected surfaces. Both degradation profiles for the deprotected polymers were similar to the second stage profile of the protected polymers, which was again hypothesized to be due to degradation of the polymer backbone. Onset degradation temperature of 438 °C was found for para-substituted deprotected polymer and 455 °C for meta-substituted deprotected polymer. First derivative of the degradation profiles showed 493 °C for parasubstituted deprotected polymer and 500 °C for meta-substituted deprotected polymer (**Figure 6**). The meta- and para-substituted deprotected polymer-modified Stöber silica particles were also characterized using TEM. Images of these systems showed a decrease in film thickness to 11 ± 5 nm and 11 ± 3 nm for the para- and meta-substituted brushes, respectively (**Figure 7**). This decrease in thickness was also observed with the polymers on the flat wafers but was more pronounced for the flat surfaces compared to the Stöber silica particles. The TEM images of the deprotected polymers also indicated that there was an increase in the surface roughness of the polymer after the deprotection reaction. This increased surface roughness is hypothesized to be

due to clumping of the polymer chains because of hydrogen bonding along the backbone of the

surfaces (Figure 5), which also show the presence of regular surface more features after the deprotection reaction. Similar to the protected polymer brush particles, the deprotected polymers were degrafted and characterized using FTIR spectroscopy. **FTIR** spectroscopy confirmed that after the deprotection reaction characteristic amide proton

polymers. These images also

correlate well to the AFM

images of the deprotected

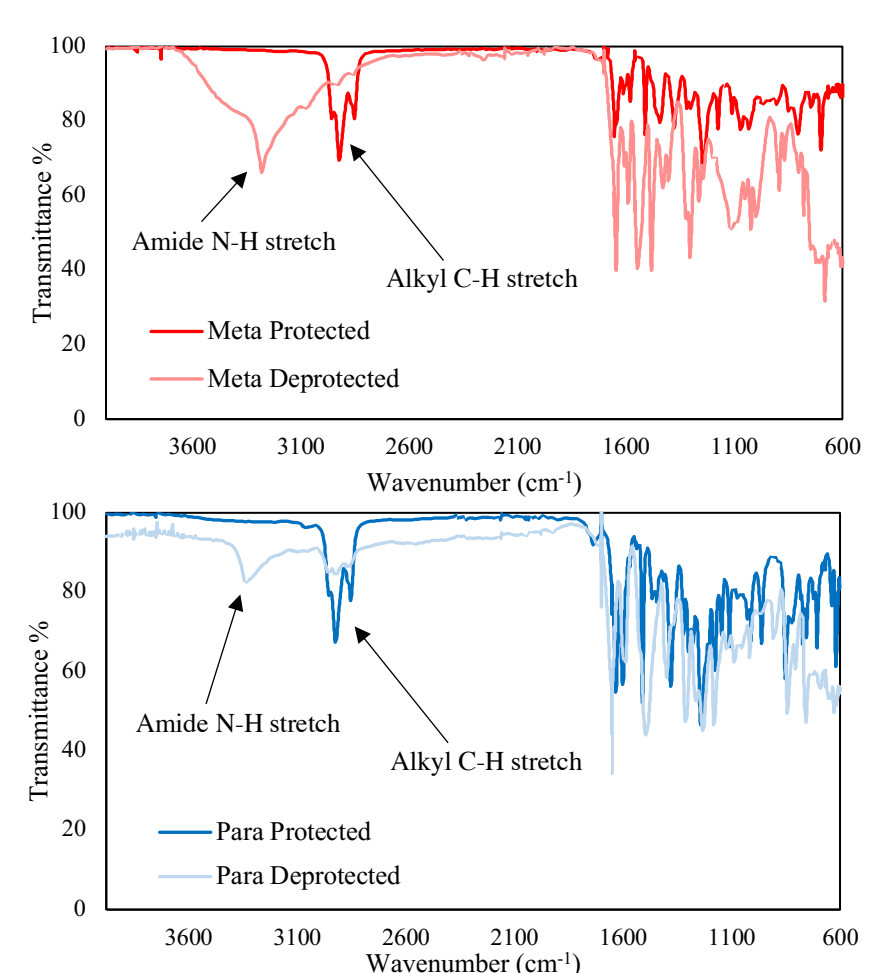


Figure 8. FTIR spectra comparing the protected and deprotected aromatic polyamides for both the para- (bottom) and meta- (top) substituted polymers degrafted from Stöber silica.

peak was seen at 3300 cm⁻¹ along with reduced alkyl side chain C-H stretches and bends at 2850 and 2930 cm⁻¹ (**Figure 8**). Due to the insolubility of the para-substituted deprotected polymer, NMR characterization was only performed on the meta-substituted deprotected polymer. NMR of the meta-substituted deprotected polymer showed a 95% deprotection efficiency, which is similar

to the solution deprotection results of 94% using the same benzyl methyl NMR peak compared to the amide proton peak.

Nanomechanical Analysis Using AFM

The physical properties of thin polymer films can play a crucial part in the performance of modified surfaces. In particular, there has been interest in tailoring the chemical robustness, mechanical strength, and functionality of polymer films for application in areas that include membranes, high performance coatings, lubrication, and adhesion. As such, in order to determine whether the introduction of hydrogen bonding along the polymer backbone improves the mechanical properties of the brushes, AFM was used to obtain force curves for each surface in order to determine the Young's modulus of the polymer brushes. To the best of our knowledge this is the first example of force measurements of fully aromatic polyamides covalently attached to a substrate.

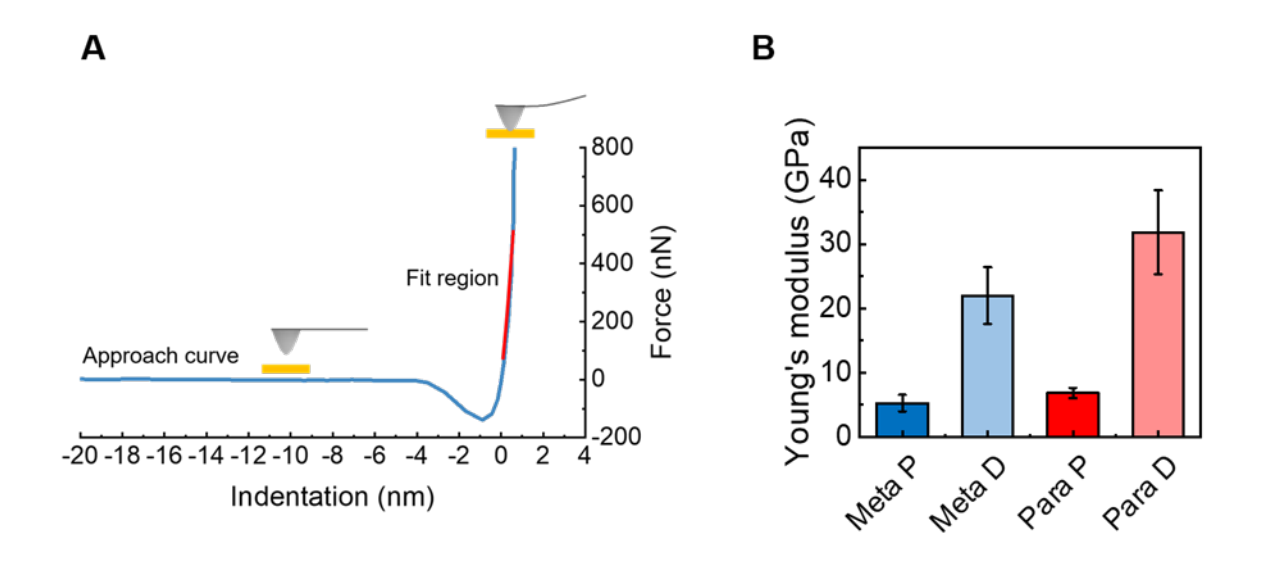


Figure 9. (A) Representative approach force-distance curve for the determination of Young's modulus. (B) Young's modulus of the different polymer brushes on flat wafers. Meta P: meta-

substituted protected; Meta D: meta-substituted deprotected; Para P: para-substituted protected; and Para D: para-substituted deprotected. Error bar represents the standard deviation, n = 10.

The mechanical properties of the different polymer brush samples were measured from forcedisplacement curves using AFM (Figure 9A). The obtained curves were fitted to eq. 1 to obtain Young's modulus values for each of the brushes (Figure 9B). These results demonstrate that removal of the protecting side chain for either the meta-substituted or para-substituted brushes resulted in a dramatic increase in the Young's modulus values. The meta-substituted brush increased from approximately 5 GPa to almost 22 GPa and the para-substituted brush from 6 GPa to almost 32 GPa. It is hypothesized that the improved modulus results from the introduction of hydrogen bonding along the backbone after the deprotection reaction. In addition, the parasubstituted deprotected brush had a higher Young's modulus than the meta-substituted brush after deprotection, which was expected due to the more linear chains with para-substitution. The Young's moduli of the deprotected aromatic polyamide brushes in this study (~20–30 GPa) are some of the highest values reported for polymer brushes and have not been previously reported for similar systems prepared using the MLD technique.¹⁷ To provide context for these values, they are a significantly higher than that reported for the thin aromatic polyamide layer used in reverse osmosis membranes (~2 GPa).62 To further provide a comparison for the Young's modulus values obtained for the aromatic polyamide brushes synthesized in this study, an aromatic polyamide film was prepared using a previously reported interfacial polymerization technique with trimesoyl chloride and meta-phenylenediamine as the monomers. 63 This film was isolated on a silica wafer and the Young's modulus measure using the same method to that used for the polymer brushes. Analysis of this aromatic polyamide film yielded a Young's modulus value of 2.0 ± 0.5 GPa, which further demonstrates the tremendous potential of these polymer brush films.

Conclusion

Aromatic polyamides are considered high performance engineering polymers due to their high heat stability, excellent chemical stability, and exceptional strength. Aromatic polyamides have very seldom been utilized for surface applications however due to the relative insolubility of these polymers in common organic solvents rendering application of these polymer to surfaces difficult. However, due to these excellent properties, high surface strength polymer films have been predicted for polymers with rigid rod backbones making these aromatic polyamides an ideal candidate to be explored. Surface initiated aromatic polyamide polymer brushes were grown from flat silicon wafers and high surface area silica particles surfaces using the newly developed surfaceinitiated substituent effect CGC polymerization method. Protecting side chains on the monomer structures were utilized to allow for deprotection after polymerization and introduce hydrogen bonding alone the backbone of the polymer. The polymerization was first examined in solution to establish the optimal polymerization conditions for the meta- and para-substituted benzyl ether protected monomers. The resultant solution polymers were then deprotected, showing high deprotection efficiency and the introduction of hydrogen bonding between chains. These results were transferred to surface-initiated polymerizations via the preparation and deposition of a new initiator system on both flat and curved surfaces. The surface-initiated polymerizations produced well defined, thick polymer brushes from both the meta- and para-substituted protected monomers. The protecting side chains on these polymer brushes were also successfully removed. TEM demonstrated a high grafting density for both the meta- and para-substituted systems, showing both were in the polymer brush regime. Finally, AFM was used to show the outstanding Young's modulus values obtained for the polymer brushes after removal of the protecting side chain introduces hydrogen bonding to the polymer backbone.

Associated Content

Supporting information

Experimental procedures for initiator and monomers, NMR spectra, and FTIR spectra

Author Information

Corresponding Authors *E-mail – sboyes@gwu.edu (SGB); xitongliu@email.gwu.edu (XL).

Notes

The authors declare no competing financial interest.

Author Contributions

The manuscript was written through contributions of all authors. All authors have given approval to the final version of the manuscript.

Funding Sources

SGB, CJR, RJD, and MDS gratefully acknowledge the support of this work by the National Science Foundation under grant CHE MSN #1807863. SGB and XL gratefully acknowledge the support of this work by The George Washington University through the Cross-Disciplinary Research Fund.

Acknowledgements

SGB, RJD, and CJR gratefully acknowledge the support of this by The George Washington University Chemistry Department.

Abbreviations

AFM. Atomic force microscopy; ATR, attenuated total reflectance; CGC, chain growth condensation: MDMS-Amide-P, phenyl 4-((3-(dimethoxy(methyl)silyl)propyl)(methyl)carbamoyl)benzoate; DCM, dichloromethane; M.p. melting deposition; point; MLD, molecular laver DMA-P, phenyl 4-(dimethylcarbamoyl)benzoate; DMAc, dimethylacetamide; DMSO, dimethylsulfoxide; DMT, Derjaguin-Muller-Toporov; DP, degree of polymerization; FT-IR, fourier-transform infrared spectroscopy; GATR, grazing-angle attenuated total reflextance; GPC, gel-permeation chromatography; LiHMDS, lithium bis(trimethylsilyl)amide; meta-OOB-P-AB, phenyl 3-((4-(octyloxy)benzyl)amino)benzoate; mLbL, molecular layer by layer; NMR, nuclear magnetic resonance; para-OOB-P-AB, phenyl 4-((4-(octyloxy)benzyl)amino)benzoate; PDI, polydispersity index; RO, reverse osmosis; TEA, triethylamine; TEM, transmission electron microscope; TEOS, tetraethyl orthosilicate; TFA, trifluoroacetic acid; TGA, thermogravimetric analysis; THF, tetrahydrofuran.

References

- (1) Reglero Ruiz, J. A.; Trigo-López, M.; García, F. C.; García, J. M. Functional Aromatic Polyamides. Polymers (Basel). 2017, 9 (9). https://doi.org/10.3390/polym9090414.
- (2) García, J. M.; García, F. C.; Serna, F.; de la Peña, J. L. High-Performance Aromatic Polyamides. Prog. Polym. Sci. 2010, 35 (5), 623–686. https://doi.org/10.1016/j.progpolymsci.2009.09.002.

- (3) Kato, T.; Mizoshita, N.; Kishimoto, K. Functional Liquid-Crystalline Assemblies: Self-Organized Soft Materials. Angew. Chemie Int. Ed. 2006, 45 (1), 38–68. https://doi.org/10.1002/anie.200501384.
- (4) Chae, H. G.; Kumar, S. Rigid-Rod Polymeric Fibers. J. Appl. Polym. Sci. 2006, 100 (1), 791–802. https://doi.org/10.1002/app.22680.
- (5) Werber, J. R.; Osuji, C. O.; Elimelech, M. Materials for Next-Generation Desalination and Water Purification Membranes. Nat. Rev. Mater. 2016, 1 (5), 16018. https://doi.org/10.1038/natrevmats.2016.18.
- (6) Ghosh, A. K.; Bindal, R. C.; Prabhakar, S.; Tewari, P. K. Composite Polyamide Reverse Osmosis (RO) Membranes Recent Developments and Future Directions. 2011, No. 321, 43–51.
- (7) Asadollahi, M.; Bastani, D.; Musavi, S. A. Enhancement of Surface Properties and Performance of Reverse Osmosis Membranes after Surface Modification: A Review. Desalination 2017, 420 (December 2016), 330–383. https://doi.org/10.1016/j.desal.2017.05.027.
- (8) Bera, D.; Chatterjee, R.; Banerjee, S. Aromatic Polyamide Nonporous Membranes for Gas Separation Application. E-Polymers 2021, 21 (1), 108–130. https://doi.org/10.1515/epoly-2021-0016.
- (9) Idarraga-Mora, J. A.; O'Neal, A. D.; Pfeiler, M. E.; Ladner, D. A.; Husson, S. M. Effect of Mechanical Strain on the Transport Properties of Thin-Film Composite Membranes Used in Osmotic Processes. J. Memb. Sci. 2020, 615 (February), 118488. https://doi.org/10.1016/j.memsci.2020.118488.

- (10) Reese, C. J.; Boyes, S. G. New Methods in Polymer Brush Synthesis: Non-Vinyl-Based Semiflexible and Rigid-Rod Polymer Brushes. Prog. Polym. Sci. 2021, 114, 101361. https://doi.org/10.1016/j.progpolymsci.2021.101361.
- (11) Senkovskyy, V.; Senkovska, I.; Kiriy, A. Surface-Initiated Synthesis of Conjugated Microporous Polymers: Chain-Growth Kumada Catalyst-Transfer Polycondensation at Work. ACS Macro Lett. 2012, 1 (4), 494–498. https://doi.org/10.1021/MZ200204G/SUPPL_FILE/MZ200204G_SI_001.PDF.
- (12) Wijmans, C. M.; Leermakers, F. A. M.; Fleer, G. J. Chain Stiffness and Bond Correlations in Polymer Brushes. J. Chem. Phys. 1994, 101 (9), 8214–8223. https://doi.org/10.1063/1.468206.
- (13) Zhao, B.; Brittain, W. Polymer Brushes: Surface-Immobilized Macromolecules. Prog. Polym. Sci. 2000, 25 (5), 677–710. https://doi.org/10.1016/S0079-6700(00)00012-5.
- (14) Morse, D. C.; Fredrickson, G. H. Semiflexible Polymers near Interfaces. Phys. Rev. Lett. 1994, 73 (24), 3235–3238. https://doi.org/10.1103/PhysRevLett.73.3235.
- (15) Amoskov, V. M.; Birshtein, T. M.; Pryamitsyn, V. A. Theory of Liquid-Crystalline (LC) Polymer Brushes: Interpenetrating Brushes. Macromolecules 1998, 31 (11), 3720–3730. https://doi.org/10.1021/ma970985d.
- (16) Milchev, A.; Binder, K. Unconventional Ordering Behavior of Semi-Flexible Polymers in Dense Brushes under Compression. Soft Matter 2014, 10 (21), 3783–3797. https://doi.org/10.1039/c3sm53133c.

- (17) Adamczyk, N. M.; Dameron, A. A.; George, S. M. Molecular Layer Deposition of Poly(p-Phenylene Terephthalamide) Films Using Terephthaloyl Chloride and p-Phenylenediamine. Langmuir 2008, 24 (5), 2081–2089. https://doi.org/10.1021/la7025279.
- (18) Lomadze, N.; Perez, M.; Prucker, O.; Rühe, J.; Reinecke, H. Step-and-Repeat Assembly of Molecularly Controlled Ultrathin Polyaramide Layers. Macromolecules 2010, 43 (21), 9056–9062. https://doi.org/10.1021/ma101389p.
- (19) Johnson, P. M.; Yoon, J.; Kelly, J. Y.; Howarter, J. A.; Stafford, C. M. Molecular Layer-by-Layer Deposition of Highly Crosslinked Polyamide Films. J. Polym. Sci. Part B Polym. Phys. 2012, 50 (3), 168–173. https://doi.org/10.1002/polb.23002.
- (20) Wallas, J. M.; Welch, B. C.; Wang, Y.; Liu, J.; Hafner, S. E.; Qiao, R.; Yoon, T.; Cheng, Y. T.; George, S. M.; Ban, C. Spatial Molecular Layer Deposition of Ultrathin Polyamide to Stabilize Silicon Anodes in Lithium-Ion Batteries. ACS Appl. Energy Mater. 2019, 2 (6), 4135–4143. https://doi.org/10.1021/acsaem.9b00326.
- (21) Sundberg, P.; Karppinen, M. Organic and Inorganic–Organic Thin Film Structures by Molecular Layer Deposition: A Review. Beilstein J. Nanotechnol. 2014, 5 (1), 1104–1136. https://doi.org/10.3762/bjnano.5.123.
- (22) Chan, E. P.; Lee, J. H.; Chung, J. Y.; Stafford, C. M. An Automated Spin-Assisted Approach for Molecular Layer-by-Layer Assembly of Crosslinked Polymer Thin Films. Rev. Sci. Instrum. 2012, 83 (11), 114102. https://doi.org/10.1063/1.4767289.

- (23) Kwon, S. B.; Lee, J. S.; Kwon, S. J.; Yun, S. T.; Lee, S.; Lee, J. H. Molecular Layer-by-Layer Assembled Forward Osmosis Membranes. J. Memb. Sci. 2015, 488, 111–120. https://doi.org/10.1016/j.memsci.2015.04.015.
- (24) Gu, J. E.; Lee, J. S.; Park, S. H.; Kim, I. T.; Chan, E. P.; Kwon, Y. N.; Lee, J. H. Tailoring Interlayer Structure of Molecular Layer-by-Layer Assembled Polyamide Membranes for High Separation Performance. Appl. Surf. Sci. 2015, 356, 659–667. https://doi.org/10.1016/j.apsusc.2015.08.119.
- (25) Chan, E. P.; Young, A. P.; Lee, J.-H.; Stafford, C. M. Swelling of Ultrathin Molecular Layer-by-Layer Polyamide Water Desalination Membranes. J. Polym. Sci. Part B Polym. Phys. 2013, 51 (22), 1647–1655. https://doi.org/10.1002/polb.23380.
- (26) Chan, E. P.; Lee, S. C. Thickness-Dependent Swelling of Molecular Layer-by-Layer Polyamide Nanomembranes. J. Polym. Sci. Part B Polym. Phys. 2017, 55 (5), 412–417. https://doi.org/10.1002/polb.24285.
- (27) Xu, G.-R.; Wang, S.; Zhao, H.; Wu, S.; Xu, J.; Li, L.; Liu, X. Layer-by-Layer (LBL) Assembly Technology as Promising Strategy for Tailoring Pressure-Driven Desalination Membranes. J. Memb. Sci. 2015, 493, 428–443. https://doi.org/10.1016/j.memsci.2015.06.038.
- (28) Mulhearn, W. D.; Oleshko, V. P.; Stafford, C. M. Thickness-Dependent Permeance of Molecular Layer-by-Layer Polyamide Membranes. J. Memb. Sci. 2021, 618 (June 2020), 118637. https://doi.org/10.1016/j.memsci.2020.118637.

- (29) Mulhearn, W. D.; Stafford, C. M. Highly Permeable Reverse Osmosis Membranes via Molecular Layer-by-Layer Deposition of Trimesoyl Chloride and 3,5-Diaminobenzoic Acid. ACS Appl. Polym. Mater. 2021, 3 (1), 116–121. https://doi.org/10.1021/acsapm.0c01199.
- (30) Prehn, F. C.; Boyes, S. G. Surface-Initiated Chain Growth Polyaramid Brushes. Macromolecules 2015, 48 (13), 4269–4280. https://doi.org/10.1021/acs.macromol.5b00957.
- (31) Yan, J.; Bockstaller, M. R.; Matyjaszewski, K. Brush-Modified Materials: Control of Molecular Architecture, Assembly Behavior, Properties and Applications. Prog. Polym. Sci. 2020, 100, 101180/1-51. https://doi.org/10.1016/j.progpolymsci.2019.101180.
- (32) Ma, S.; Zhang, X.; Yu, B.; Zhou, F. Brushing up Functional Materials. NPG Asia Materials. Nature Publishing Group December 1, 2019, pp 1–39. https://doi.org/10.1038/s41427-019-0121-2.
- (33) Yokozawa, T.; Asai, T.; Sugi, R.; Ishigooka, S.; Hiraoka, S. Chain-Growth Polycondensation for Nonbiological Polyamides of Defined Architecture. J. Am. Chem. Soc. 2000, 122 (34), 8313–8314. https://doi.org/10.1021/ja001871b.
- (34) Yokozawa, T.; Ogawa, M.; Sekino, A.; Sugi, R.; Yokoyama, A. Chain-Growth Polycondensation for Well-Defined Aramide. Synthesis of Unprecedented Block Copolymer Containing Aramide with Low Polydispersity. J. Am. Chem. Soc. 2002, 124 (51), 15158–15159. https://doi.org/10.1021/ja021188k.
- (35) Yokozawa, T.; Ogawa, M.; Sekino, A.; Sugi, R.; Yokoyama, A. Synthesis of Well-Defined Poly(p-Benzamide) from Chain-Growth Polycondensation and Its Application to Block Copolymers. Macromol. Symp. 2003, 199 (1), 187–196. https://doi.org/10.1002/masy.200350916.

- (36) Sugi, R.; Yokoyama, A.; Furuyama, T.; Uchiyama, M.; Yokozawa, T. Inductive Effect-Assisted Chain-Growth Polycondensation. Synthetic Development from Para- to Meta-Substituted Aromatic Polyamides with Low Polydispersities. J. Am. Chem. Soc. 2005, 127 (29), 10172–10173. https://doi.org/10.1021/ja052566z.
- (37) Yokozawa, T.; Muroya, D.; Sugi, R.; Yokoyama, A. Convenient Method of Chain-Growth Polycondensation for Well-Defined Aromatic Polyamides. Macromol. Rapid Commun. 2005, 26 (12), 979–981. https://doi.org/10.1002/marc.200500109.
- (38) Yokozawa, T.; Yokoyama, A. Chain-Growth Polycondensation for Well-Defined Condensation Polymers and Polymer Architecture. Chem. Rec. 2005, 5 (1), 47–57. https://doi.org/10.1002/tcr.20032.
- (39) Yokozawa, T.; Yokoyama, A. Chain-Growth Polycondensation: The Living Polymerization Process in Polycondensation. Prog. Polym. Sci. 2007, 32 (1), 147–172. https://doi.org/10.1016/j.progpolymsci.2006.08.001.
- (40) Yokoyama, A.; Yokozawa, T. Converting Step-Growth to Chain-Growth Condensation Polymerization. Macromolecules 2007, 40 (12), 4093–4101. https://doi.org/10.1021/ma061357b.
- (41) Yokozawa, T.; Yokoyama, A. Chain-Growth Condensation Polymerization for the Synthesis of Well-Defined Condensation Polymers and π-Conjugated Polymers. Chem. Rev. 2009, 109 (11), 5595–5619. https://doi.org/10.1021/cr900041c.
- (42) Yokozawa, T.; Ohta, Y. Scope of Controlled Synthesis via Chain-Growth Condensation Polymerization: From Aromatic Polyamides to π-Conjugated Polymers. Chem. Commun. 2013, 49 (75), 8281–8310. https://doi.org/10.1039/c3cc43603a.

- (43) Yokozawa, T.; Ohta, Y. Transformation of Step-Growth Polymerization into Living Chain-Growth Polymerization. Chem. Rev. 2016, 116 (4), 1950–1968. https://doi.org/10.1021/acs.chemrev.5b00393.
- (44) Prehn, F. C.; Etz, B. D.; Reese, C. J.; Vyas, S.; Boyes, S. G. Chain-growth Polycondensation via the Substituent Effect: Investigation of the Monomer Structure on Synthesis of Poly(N-octyl-benzamide). J. Polym. Sci. 2020, 58 (17), 2389–2406. https://doi.org/10.1002/pol.20200435.
- (45) Prehn, F. C.; Etz, B. D.; Price, D.; Trainor, A.; Reese, C. J.; Vyas, S.; Boyes, S. G. Chaingrowth Polycondensation via the Substituent Effect: Investigation in to the Role of Initiator and Base on the Synthesis of Poly(N -octyl Benzamide). J. Polym. Sci. 2020, 58 (17), 2407–2422. https://doi.org/10.1002/pol.20200436.
- (46) Ohta, Y.; Karasawa, M.; Niiyama, T.; Yokoyama, A.; Yokozawa, T. Synthesis of Well-Defined, Soluble Poly(3-Alkyl-4-Benzamide) by Chain-Growth Condensation Polymerization. J. Polym. Sci. Part A Polym. Chem. 2014, 52 (3), 360–365. https://doi.org/10.1002/pola.27008.
- (47) Wójcik, A. J.; Wolski, K.; Zapotoczny, S. Double-Stranded Surface-Grafted Polymer Brushes with Ladder-like Architecture. Eur. Polym. J. 2021, 155, 110577. https://doi.org/10.1016/j.eurpolymj.2021.110577.
- (48) Lin, J.; Sherrington, D. C. Recent Developments in the Synthesis, Thermostability and Liquid Crystal Properties of Aromatic Polyamides. In Polymer Synthesis; Springer-Verlag: Berlin/Heidelberg, 1994; Vol. 111, pp 177–219. https://doi.org/10.1007/BFb0024129.

- (49) Ducker, W. A.; Senden, T. J.; Pashley, R. M. Measurement of Forces in Liquids Using a Force Microscope. Langmuir 1992, 8, 1831–1836.
- (50) Ohishi, T.; Sugi, R.; Yokoyama, A.; Yokozawa, T. A Variety of Poly(m-Benzamide)s with Low Polydispersities from Inductive Effect-Assisted Chain-Growth Polycondensation. J. Polym. Sci. Part A Polym. Chem. 2006, 44 (17), 4990–5003. https://doi.org/10.1002/pola.21616.
- (51) Ohta, Y.; Niiyama, T.; Yokoyama, A.; Yokozawa, T. Chain-Growth Condensation Polymerization Approach to Synthesis of Well-Defined Polybenzoxazole: Importance of Higher Reactivity of 3-Amino-4-Hydroxybenzoic Acid Ester Compared to 4-Amino-3-Hydroxybenzoic Acid Ester. J. Polym. Sci. Part A Polym. Chem. 2014, 52 (12), 1730–1736. https://doi.org/10.1002/pola.27174.
- (52) Lee, S. Y.; Kim, J. S.; Lim, S. H.; Jang, S. H.; Kim, D. H.; Park, N. H.; Jung, J. W.; Choi, J. The Investigation of the Silica-Reinforced Rubber Polymers with the Methoxy Type Silane Coupling Agents. Polymers (Basel). 2020, 12 (12), 1–14. https://doi.org/10.3390/polym12123058.
- (53) Matyjaszewski, K. Introduction to Living Polymeriz. Living and/or Controlled Polymerization. J. Phys. Org. Chem. 1995, 8 (4), 197–207. https://doi.org/10.1002/poc.610080403.
- (54) Barbey, R.; Lavanant, L.; Paripovic, D.; Schüwer, N.; Sugnaux, C.; Tugulu, S.; Klok, H. Polymer Brushes via Surface-Initiated Controlled Radical Polymerization: Synthesis, Characterization, Properties, and Applications. Chem. Rev. 2009, 109 (11), 5437–5527. https://doi.org/10.1021/cr900045a.

- (55) Shircliff, R. A.; Stradins, P.; Moutinho, H.; Fennell, J.; Ghirardi, M. L.; Cowley, S. W.; Branz, H. M.; Martin, I. T. Angle-Resolved XPS Analysis and Characterization of Monolayer and Multilayer Silane Films for DNA Coupling to Silica. Langmuir 2013, 29 (12), 4057–4067. https://doi.org/10.1021/la304719y.
- (56) Tripp, C. P.; Hair, M. L. Chemical Attachment of Chlorosilanes to Silica: A Two-Step Amine-Promoted Reaction. J. Phys. Chem. 1993, 97 (21), 5693–5698. https://doi.org/10.1021/j100123a038.
 - (57) Salazar, Noel B.; Graburn, N. Handbook of Ellipsometry; 2005.
- (58) Matyjaszewski, K.; Miller, P. J.; Shukla, N.; Immaraporn, B.; Gelman, A.; Luokala, B. B.; Siclovan, T. M.; Kickelbick, G.; Vallant, T.; Hoffmann, H.; Pakula, T. Polymers at Interfaces: Using Atom Transfer Radical Polymerization in the Controlled Growth of Homopolymers and Block Copolymers from Silicon Surfaces in the Absence of Untethered Sacrificial Initiator. Macromolecules 1999, 32 (26), 8716–8724. https://doi.org/10.1021/ma991146p.
- (59) Stöber, W.; Fink, A.; Bohn, E. Controlled Growth of Monodisperse Silica Spheres in the Micron Size Range. J. Colloid Interface Sci. 1968, 26 (1), 62–69. https://doi.org/10.1016/0021-9797(68)90272-5.
- (60) Cheesman, B. T.; Neilson, A. J. G.; Willott, J. D.; Webber, G. B.; Edmondson, S.; Wanless, E. J. Effect of Colloidal Substrate Curvature on pH-Responsive Polyelectrolyte Brush Growth. Langmuir 2013, 29 (20), 6131–6140. https://doi.org/10.1021/la4004092.
- (61) Brown, J. R.; Ennis, B. C. Thermal Analysis of Nomex® and Kevlar® Fibers. Text. Res.
 J. 1977, 47 (1), 62–66. https://doi.org/10.1177/004051757704700113.

- (62) Zhang, X.; Cahill, D. G.; Coronell, O.; Mariñas, B. J. Absorption of Water in the Active Layer of Reverse Osmosis Membranes. J. Memb. Sci. 2009, 331 (1–2), 143–151.
- (63) Ma, X-. H.; Yao, D-. K.; Yang, Z.; Guo, H.; Xu, Z-. L.; Tang, C. Y.; Elimelech, M. Nanofoaming of Polyamide Desalination Membranes to Tune Permeability and Selectivity. Environ. Sci. Technol. Lett. 2018, 5, 123–130.